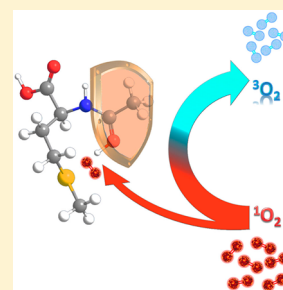


Collision Dynamics of Protonated *N*-Acetylmethionine with Singlet Molecular Oxygen ($a^1\Delta_g$): The Influence of the Amide Bond and Ruling Out the Complex-Mediated Mechanism at Low Energies

Wenchao Lu, Fangwei Liu, Rifat Emre, and Jianbo Liu*

Department of Chemistry and Biochemistry, Queens College and the Graduate Center of the City University of New York, 65-30 Kissena Boulevard, Queens, New York 11367, United States

ABSTRACT: It has been proposed (*J. Phys. Chem. B* 2011, 115, 2671) that the ammonium group is involved in the gas-phase reaction of protonated methionine (MetH^+) with singlet oxygen $^1\text{O}_2$, yielding hydrogen peroxide and a dehydro compound of MetH^+ where the $-\text{NH}_3^+$ transforms into cyclic $-\text{NH}_2^-$. For the work reported, the gas-phase reaction of protonated *N*-acetylmethionine (Ac-MetH^+) with $^1\text{O}_2$ was examined, including the measurements of reaction products and cross sections over a center-of-mass collision energy (E_{col}) range from 0.05 to 1.0 eV using a guided-ion-beam apparatus. The aim is to probe how the acetylation of the ammonium group affects the oxidation chemistry of the ensuing Ac-MetH^+ . Properties of intermediates, transition states, and products along the reaction coordinate were explored using density functional theory calculations and Rice–Ramsperger–Kassel–Marcus (RRKM) modeling. Direct dynamics trajectory simulations were carried out at E_{col} of 0.05 and 0.1 eV using the B3LYP/4-31G(d) level of theory. In contrast to the highly efficient reaction of $\text{MetH}^+ + ^1\text{O}_2$, the reaction of $\text{Ac-MetH}^+ + ^1\text{O}_2$ is extremely inefficient, despite there being exoergic pathways. Two product channels were observed, corresponding to transfer of two H atoms from Ac-MetH^+ to $^1\text{O}_2$ (H2T), and methyl elimination (ME) from a sulfone intermediate complex. Both channels are inhibited by collision energies, becoming negligible at $E_{\text{col}} > 0.2$ eV. Analysis of RRKM and trajectory results suggests that a complex-mediated mechanism might be involved at very low E_{col} , but direct, nonreactive collisions prevail over the entire E_{col} range and physical quenching of $^1\text{O}_2$ occurs during the early stage of collisions.



I. INTRODUCTION

Electronically excited singlet molecular oxygen $\text{O}_2[a^1\Delta_g]$ has a characteristic chemistry in which molecules are oxygenated, leading to cell death, aging, and diseases in biological systems,^{1,2} as well as destruction of the affected cells in the treatment of malignancies by photodynamic therapy.³ Proteins are the major target for $^1\text{O}_2$, with oxidative damage occurring preferentially at tryptophan (Trp), histidine (His), tyrosine (Tyr), methionine (Met), and cysteine (Cys) residues.^{1,2} Other residues are resistant to photodynamic action.

Of these five susceptible residues, Met represents a special case in which oxidative modification of Met can be repaired by methionine sulfoxide reductases that catalyze the reduction of methionine sulfoxide residues back to Met residues.^{4,5} Consequently, Met residues act as an antioxidant pool, and the increase of oxidized Met residues in proteins may reflect an increase of $^1\text{O}_2$ generation, decrease of oxidant scavengers, or loss of methionine sulfoxide reductases and other reducing equivalents involved. For this reason, Met oxidation has been extensively investigated. Most Met oxidation experiments were carried out in solution where $^1\text{O}_2$ was generated by photosensitization, i.e., light was used to create an excited state of a sensitizer, which in turn transferred its excitation energy to ground-state O_2 to generate $^1\text{O}_2$.⁶ Sensitized photooxidation of Met yielded various products.^{1,2,7–14} The reaction initially formed a persulfoxide intermediate.¹⁵ The dark reaction of the persulfoxide is pH dependent and appears to be sensitive to

solvent composition and polarity.¹⁶ Experiments in solution were further interfered by type I (free-radical-mediated)^{17,18} photooxidation mechanism, and other reactive species such as $\cdot\text{OH}$ and sensitizer radicals may have contributed to Met oxidation as well.

To avoid the complexities and interference arising from solution-phase photooxidation experiments and simplify the interpretation of Met oxidation mechanism, we have studied the $^1\text{O}_2$ oxidation of protonated Met (MetH^+) in the gas phase using a chemically generated, clean $^1\text{O}_2$ source.¹⁹ Investigating biomolecules in the gas phase allows us to observe single molecules separated from bulk solution. In this way, intrinsic reactivity of Met can be distinguished from solvent effects.

Oxidation of free Met might be used as an initial approximation for the $^1\text{O}_2$ damage of Met-containing proteins. However, an important question is, “can the oxidation mechanism derived from free Met be straightforwardly extrapolated to the Met residues binding to complex biological assemblies, or should better model systems be sought?” Peptide linkage is a key facet in the structure of proteins, and research on influences of the peptide linkage on amino acid oxidation produced diverse results.^{12,20–23} For instance, photooxidation of dipeptide Tyr-Gly had a reaction rate and oxidation products

Received: January 22, 2014

Revised: March 17, 2014

Published: March 19, 2014

similar to that of free Tyr; conversely, photooxidation of Gly-Tyr, where the amino group of Tyr is engaged in formation of the peptide bond, was inhibited and formed different products.^{12,22} Different than the case of Tyr, dipeptides Gly-Trp and Trp-Gly both produced *N*-formylkynurenine (or similar products) upon photooxidation as free Trp, and the reactions could be kinetically modeled as a mixture of Trp + Gly with low, if any, influence of the peptide bond on the oxidation kinetics.^{21,22} A similar scenario occurred in photooxidation of His and its dipeptides with Gly (i.e., His-Gly and Gly-His).²⁴ These findings emphasize the importance of adjacent functional groups as well as nearby aliphatic amino acid residues on the propensity of oxidizable residues to photodynamic action.

Following this line, we have extended gas-phase ¹O₂ experiment to a simple model dipeptide compound containing Met—protonated *N*-acetylmethionine (Ac-MetH⁺), attempting to determine how the susceptibility of Met to ¹O₂ (e.g., chemical vs physical quenching of ¹O₂) changes as a simple modification is made at the *N*-terminal of Met. A few works exist for photooxidation of *N*-acetylated Met and the dipeptide of Met with Gly,^{9,24–26} but without many mechanistic details. In the present work, ion scattering methods were employed to examine the collisions of Ac-MetH⁺ with ¹O₂, including measurements of reaction products and cross sections over a wide range of collision energies (*E*_{col}). Density functional theory (DFT) electronic structure calculations were used to explore intermediate complexes and transition states along the reaction coordinate, and Rice–Ramsperger–Kassel–Marcus (RRKM) theory²⁷ was then used to predict intermediate properties. Finally, quasi-classical direct dynamics trajectory simulations were used to provide additional mechanistic insights.

II. EXPERIMENTAL AND COMPUTATIONAL METHODS

A. Ion–Molecule Scattering Experiment. The experiment was carried out on a home-built electrospray-ionization (ESI)²⁸ guided-ion-beam tandem mass spectrometer that has been described previously, along with operation, calibration, and data analysis procedures.^{19,29–33} The apparatus consists of an ion source, radio frequency (rf), hexapole ion guide, quadrupole mass filter, rf octopole ion guide surrounded by a scattering cell, second quadrupole mass filter, and a pulse-counting detector. Both quadrupole mass filters use Extrel 9.5 mm trifilter rods and were operated at 2.1 MHz with a detectable mass/charge (*m/z*) range of 1–500.

A solution of Ac-MetH⁺ was prepared in methanol/water (1:1 vol ratio) containing 5×10^{-4} M Ac-Met ($\geq 98.5\%$, Fluka) and an equimolar amount of hydrochloric acid (Riedel-de Haën). The solution was electrosprayed into an ambient atmosphere at a flow rate of 0.03 mL/h. The electrospray voltage was set at 2430 V relative to ground. Positively charged droplets formed from electrospray were fed into the ion source chamber through a heated desolvation capillary. The capillary was biased at 73 V relative to ground and heated to 130 °C. Liquid droplets underwent desolvation as they passed through the heated capillary, converting to gas-phase ions in the source chamber. A skimmer with an orifice diameter of 0.99 mm is located 3 mm from the capillary end, separating the ion source chamber and the hexapole ion guide. The skimmer was biased at 17 V relative to ground, and the electrical field between the capillary and skimmer removed the remaining solvent molecules attached to ions by collision-induced desolvation.

Ions emerging from the skimmer were passed into the hexapole ion guide, which was maintained at a pressure of 22 mTorr, and underwent collisional focusing and cooling. The internal energy of the primary ions was determined to have a Maxwell–Boltzmann distribution at ~ 310 K.²⁹ Ions subsequently passed into the quadrupole mass filter to remove other ionic species except Ac-MetH⁺. Reactant ions Ac-MetH⁺ were collected at the exit of the mass filter and injected into the octopole ion guide. The octopole passes through a scattering cell containing ¹O₂ gas. The cell pressure was measured by a Baratron capacitance manometer (MKS 690 head and 670 signal conditioner). The ion guide trapped ions in the radial direction, minimizing losses of the reactant and product ions resulting from scattering off ¹O₂ molecules. After passing through the scattering cell, unreacted Ac-MetH⁺ and product ions drifted to the end of the octopole, mass analyzed by the second mass filter, and counted.

The initial kinetic energy distribution of the Ac-MetH⁺ ion beam was determined using a retarding potential analysis,³⁴ i.e., measuring the intensity of the ion beam while sweeping the DC bias voltage applied to the octopole. The DC bias voltage also allowed control of the kinetic energy (*E*_{lab}) of reactant ions in the laboratory frame, thereby setting the collision energy (*E*_{col}) between reactant ions and ¹O₂ in the center-of-mass frame using $E_{\text{col}} = E_{\text{lab}} m_{\text{neutral}} / (m_{\text{ion}} + m_{\text{neutral}})$, where *m*_{neutral} and *m*_{ion} are the masses of ¹O₂ and Ac-MetH⁺, respectively. The Ac-MetH⁺ ion beam intensity was 8×10^5 ion/s and constant within 10%. The initial kinetic energy of the ion beam was around 0.95 eV, and the energy spread was 0.7 eV. This corresponds to an energy spread of 0.1 eV in the center-of-mass frame for the collisions of Ac-MetH⁺ with ¹O₂. Reaction cross sections as a function of *E*_{col} were calculated from the ratio of product and reactant ion intensities (under single ion–molecule collision conditions), ¹O₂ pressure, and the calibrated effective length of the scattering cell.²⁹

¹O₂ was generated by the reaction of H₂O₂ + Cl₂ + 2KOH → O₂(X³Σ_g[−] and a¹Δ_g) + 2KCl + 2H₂O. We adopted this technique from Viggiano's group³⁵ with some modifications.^{19,30} Briefly, 13 mL of 8 M KOH (>85%, Fisher) solution was added to 20 mL of aqueous H₂O₂ (35 wt %, Acros Organics) in a sparger held at −19 °C by a recirculating chiller, and the resulting H₂O₂/KOH mixture was degassed. A He flow (research grade, T. W. Smith) was introduced to the slushy mixture at a flow rate of 50 sccm to prevent freezing of the mixture. Cl₂ ($\geq 99.5\%$, Sigma-Aldrich), at a flow rate of 2.6 sccm, was then mixed with He in a gas proportioner and bubbled through the H₂O₂/KOH solution. Cl₂ completely reacted with H₂O₂ to form ground-state and excited O₂.³⁶ Resulting gas products passed through a cold trap kept at −70 °C to remove water vapor. Only ³O₂, ¹O₂, and He remained in the downstream gas.

Before leaking into the scattering cell, the gases flowed through an emission cell for detection of ¹O₂ emission (a¹Δ_g → X³Σ_g[−], *ν* = 0–0) at 1270 nm.³⁷ The emission cell was continuously evacuated to 15 Torr using a pressure relay. This is to reduce the residence time and hence the wall quenching of ¹O₂ inside the cold trap, tubing, and emission cell. Emission from the cell was collimated by a plano-convex lens, and passed through an optical chopper (SRS model SR540) and a 5 nm bandwidth interference filter centered at 1270 nm. Chopped emission was focused into a thermoelectrically cooled InGaAs detector (Newport 71887 detector with 77055 TE-cooler controller), and the signal was processed by a lock-in amplifier

(SRS model SR830). To determine absolute $^1\text{O}_2$ concentration, the detection system was calibrated using the known reaction rate for $\text{HS}^- + ^1\text{O}_2 \rightarrow \text{SO}^- + \text{OH}$.³¹ $^1\text{O}_2$ pressure in the scattering cell is the product of the total gas pressure of O_2/He in the scattering cell, the percentage of Cl_2 in the Cl_2/He flow, and the $^1\text{O}_2$ concentration ($\sim 10\%$) in the oxygen product.

The pressure of O_2/He in the scattering cell was set at 0.30 mTorr, which contained 5% O_2 (including $^1\text{O}_2$ and $^3\text{O}_2$). The collision cross section (σ_{col}) for $\text{Ac-MetH}^+ + \text{O}_2$, taken as the greater of ion-induced dipole capture cross section (σ_{capture})³⁸ and hard-sphere cross section ($\sigma_{\text{hard-sphere}}$, calculated from the orientation-averaged contact radii of the reactants), is 79–95 Å² in the E_{col} range of 0.05–1.0 eV. Under these conditions, the probability of Ac-MetH^+ ions undergoing a single collision with O_2 is 2.3%, and that of double collisions is <0.1%. Ac-MetH^+ also collided with He, with a single-collision probability of 17% and a double-collision probability of 4%. However, the heavy ion–light neutral combination makes these collisions insignificant compared to those with O_2 .

The experiment was repeated several times, and each time we cycled through different collision energies. The concentration of $^1\text{O}_2$ was monitored continuously during the experiment, and concentration variation (controlled to within 20%) was corrected for in calculating reaction cross sections. The results presented are averages of several complete data sets. Based on the reproducibility of the cross section measurements, the relative error is <20%. To check the reactivity of Ac-MetH^+ toward ground-state O_2 and He, control experiments were performed under the same conditions except that Cl_2 gas used for the $^1\text{O}_2$ generator was replaced by oxygen gas at the same flow rate.

B. Electronic Structure Calculations, RRKM Modeling, and Direct Dynamics Simulations. Geometries of the reactants, intermediates, transition states (TSs), and products along the reaction coordinate were optimized using Gaussian 09,³⁹ at the B3LYP level of theory with various basis sets including 6-31+G(d), 6-311++G(d,p), and aug-cc-pVTZ. All of the TSs found were verified as first-order saddle points by frequency calculations, and the vibrational mode with an imaginary frequency corresponds to the associated reaction pathway. When necessary, intrinsic reaction coordinate (IRC) calculations and/or relaxed potential energy surface scans were performed to determine which minima are connected by a TS. DFT-calculated vibrational frequencies and zero-point energies (ZPEs) were scaled by a factor of 0.952 and 0.977, respectively.⁴⁰ To obtain more accurate energies for TSs, single-point calculations were done at both MP2/aug-cc-pVTZ and B3LYP/aug-cc-pVTZ levels of theory using the DFT-optimized geometries, and the results shown are for whichever gave the lower energy. The RRKM rate and density of states (DOS) were calculated with the program of Zhu and Hase,⁴¹ using its direct state count algorithm and scaled frequencies and energetics from DFT calculations.

Direct dynamics simulations for $\text{Ac-MetH}^+ + ^1\text{O}_2$ trajectories were performed using the Venus software⁴² interfaced with Gaussian 09. Considering the accuracy and the computational cost, the B3LYP/4-31G(d) method was chosen for trajectory simulations. The initial separation between Ac-MetH^+ and $^1\text{O}_2$ was set at 8.0 Å, with a collision impact parameter of 0.1 Å. The vibrational and rotational temperatures of both reactants were 300 K which was chosen to mimic our experiment, and quasi-classical Boltzmann sampling⁴³ was used to select their

vibrational and rotational energies. Collision energy was then added as relative translation energy.

The Hessian-based predictor–corrector algorithm⁴⁴ in Gaussian 09 was used for numerical integration of the classical equations of motion, with the Hessian matrix updated every five steps. Ensuring the system remains in the same electronic state during the trajectory integration is important for an adiabatic collision. A step size of 0.25 amu^{1/2} Bohr (corresponding to a step size of ~ 0.5 fs in trajectory time) was used for trajectories, which was small enough for SCF convergence as well as to keep the total energy constant. The initial guess of molecular orbital for each DFT calculation was obtained from the previous trajectory step, and the total energy of the system was checked during the simulation to ensure the energy was conserved to better than 10^{-4} hartree. The SCF = XQC option was adopted for the trajectory integration so that a quadratically convergent SCF method^{39,45} was used in case the usual, but much faster, first-order SCF method failed to converge within the allotted number of cycles.

Batches of trajectories (50 each) were calculated at $E_{\text{col}} = 0.05$ and 0.1 eV. All trajectories were terminated after 2500 steps or when the product separation exceeded 8.0 Å. The actual computer processing time for a trajectory ranged from 550 to 650 CPU hours on an Intel Core i7 6-core (3.2 GHz)-based Linux workstation cluster.

III. RESULTS AND DISCUSSION

A. Reaction Products and Cross Sections. Product ions of $\text{Ac-MetH}^+(m/z 192) + ^1\text{O}_2$ were observed at m/z 133, 144, 146, 174, 190, and 209 over the collision energies range of 0.05–1.0 eV. Product ions of m/z 133, 144, 146, 174 correspond to elimination of CH_3CONH_2 , CH_3SH , ($\text{H}_2\text{O} + \text{CO}$), and H_2O from CID of Ac-MetH^+ , respectively, of which m/z 144 and 174 are the dominant fragment ions. These product ions were also observed upon collisions of Ac-MetH^+ with ground-state O_2 and He with intensities increasing at high E_{col} , and therefore could be excluded from $^1\text{O}_2$ -specific reactions.

Products ions of m/z 190 and 209, on the other hand, were not observed with $^3\text{O}_2/\text{He}$ and cannot be attributed to CID products. m/z 190 corresponds to a structure of $\text{CH}_3\text{CONHCH}(\text{CO}_2\text{H})\text{CH}_2\text{CH}_2\text{SCH}_2^+$, and m/z 209 to $\text{CH}_3\text{COHNHCH}(\text{CO}_2\text{H})\text{CH}_2\text{CH}_2\text{SO}_2^+$. The $\text{CH}_3\text{CONHCH}(\text{CO}_2\text{H})\text{CH}_2\text{CH}_2\text{SCH}_2^+$ product ion was formed by transfer of two hydrogen atoms from Ac-MetH^+ to $^1\text{O}_2$ (referred to in generic form as H2T), accompanied by formation of H_2O_2 ; and $\text{CH}_3\text{COHNHCH}(\text{CO}_2\text{H})\text{CH}_2\text{CH}_2\text{SO}_2^+$ was formed by elimination of a methyl group from a sulfone intermediate complex $\text{Ac-MetH}^+\text{-SO}_2$ (referred to as ME). As discussed below, other isomers of m/z 190 and 209 are possible; however, they are less likely to form at low collision energies.

The product cross sections for H2T and ME are shown in Figure 1, as a function of the center-of-mass E_{col} . Both product channels appear to be exothermic without having any energy barriers above the reactants, and both are strongly suppressed by collision energy at low E_{col} , becoming negligible at $E_{\text{col}} > 0.2$ eV. Based on the measured total reaction cross sections, the reaction efficiency ($=\sigma_{\text{total}}/\sigma_{\text{col}}$) for $\text{Ac-MetH}^+ + ^1\text{O}_2$ is only $\sim 1\%$ at $E_{\text{col}} = 0.05$ eV and drops to 0.3% at $E_{\text{col}} = 0.1$ eV. Note that various CID channels, because of their endoergicities, do not interfere with H2T and ME at low E_{col} .

B. Comparison with Gas-Phase $\text{MetH}^+ + ^1\text{O}_2$ and Solution-Phase Photooxidation. The extremely low reac-

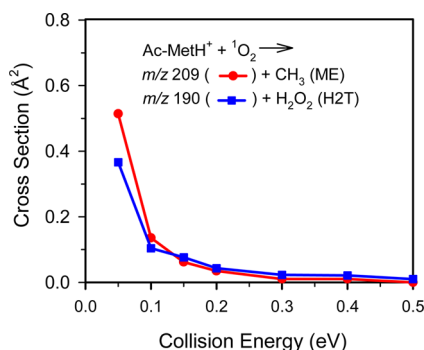


Figure 1. Product cross sections for the reaction of protonated *N*-acetylmethionine with $^1\text{O}_2$, as a function of center-of-mass collision energy.

tion efficiency for the collisions of $\text{Ac-MetH}^+ + ^1\text{O}_2$ is in sharp contrast to that of $\text{MetH}^+ + ^1\text{O}_2$.¹⁹ Gas-phase collisions of MetH^+ with $^1\text{O}_2$ lead to overwhelming formation of $\text{H}_2\text{NCH}(\text{CO}_2\text{H})\text{CH}_2\text{CH}_2\text{SCH}_2^+ + \text{H}_2\text{O}_2$ via a H2T reaction, with an efficiency of 55–82% at $E_{\text{col}} = 0.1\text{--}0.2$ eV. It follows that MetH^+ acts as a $^1\text{O}_2$ chemical probe and could be nearly quantitatively oxidized by $^1\text{O}_2$, while Ac-MetH^+ may experience the competition between chemical reaction and physical quenching (i.e., collisional deactivation without a chemical reaction taking place) of $^1\text{O}_2$, as well as possible dynamical bottleneck that suppresses the reaction.

On the other hand, gas-phase results of the low reaction efficiency for Ac-MetH^+ vs high efficiency for MetH^+ is consistent with solution-phase photooxidation results.^{24–26} The measurements of the overall $^1\text{O}_2$ quenching rate (k_{total} , based on $^1\text{O}_2$ emission) and the chemical reaction rate (k_{reaction} , based on loss of the primary amine and spectra of photolyzed compounds) indicate that only the interaction of free Met with $^1\text{O}_2$ is a pure reactive one with no physical quenching. The efficiency of the Met moiety as a chemical quencher is diminished by substitution on the amino or the carboxylic group, as occurred to Gly-Met and Met-methyl ester.²⁴ Note that blocking the amino group actually increases the overall quenching rate in solution; e.g., $k_{\text{total}} = 2.1 \times 10^{-7} \text{ M}^{-1} \text{ s}^{-1}$ for Gly-Met vs $1.3 \times 10^{-7} \text{ M}^{-1} \text{ s}^{-1}$ for Met measured in 1:1 D_2O –ethanol with $\text{pH} = 7$.²⁶ The main contribution to k_{total} is the physical quenching by Gly-Met. In other words, Gly-Met provides a mechanism that protects the Met residue against photodynamic damage.²⁴

C. Reaction Mechanism. 1. Gas-Phase Structures of Ac-MetH^+ . Ac-MetH^+ may exist in various conformations resulting from the flexibility of its structure. Also note that, unlike Met of which the amino group is the most basic site for protonation,¹⁹ the carbonyl oxygen of the *N*-acetyl group becomes the preferred protonation site for Ac-Met . This is because the charge in the ensuing $\text{HNC}=\text{OH}^+$ group can be stabilized by an ionic hydrogen bond with the side-chain sulfide group (i.e., $\text{HNC}=\text{OH}^+ \rightarrow \text{S}$) and by “amide resonance” with a protonated imine structure (i.e., $\text{HNC}=\text{OH}^+ \leftrightarrow \text{HN}^+=\text{C}-\text{OH}$).^{46,47} To find the global minimum in the Ac-MetH^+ conformational landscape, we applied a grid search method.⁴⁸ Since we are only interested in low-energy conformations, we have assumed a *syn*-configuration of the carboxylic acid group of Ac-MetH^+ . Each of the remaining torsion angles of Ac-MetH^+ was systematically rotated through 360° at 60° increments to generate all possible conformations. Every conformation so generated was subjected to geometry

optimization at the B3LYP/6-31+G* level of theory to derive the associated local minimum energy conformation. Many of the initial conformations converged to the same local minimum. These conformations were then optimized at the B3LYP/6-311++G** level of theory, resulting in a total of 14 stable conformers. Their structures and relative energies (0 K, including ZPE) with respect to conformer a, the lowest energy conformation, are summarized in Figure 2.

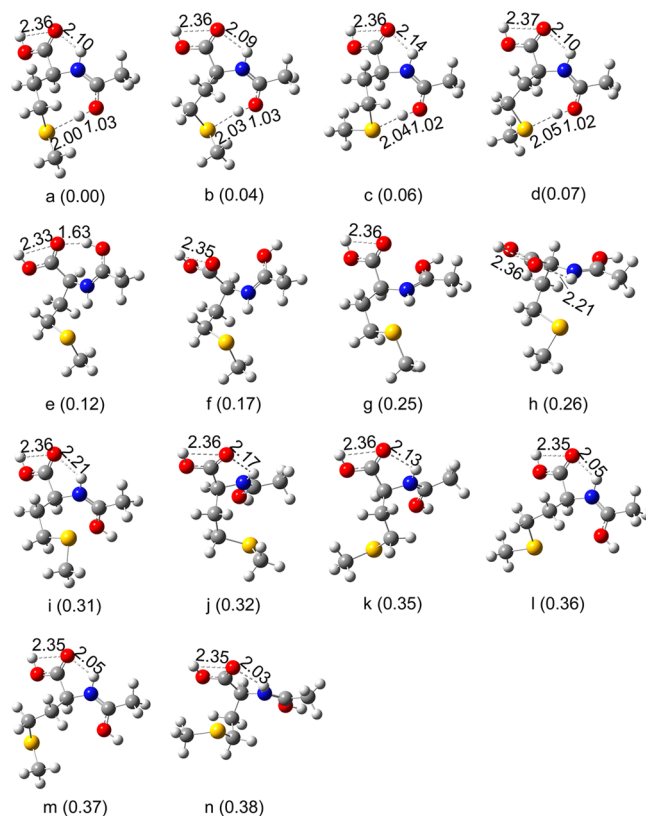


Figure 2. Low-lying conformations of protonated *N*-acetylmethionine calculated at the B3LYP/6-311++G(d,p) level of theory. Their relative energies at 0 K (including ZPE) are indicated in parentheses. The bond distances are shown in angstroms.

Conformers a–d, depicted in the top row of Figure 2, are within 0.1 eV in energy. These conformers are characterized by strong intramolecular charge complexation by the side-chain sulfide group and the C-terminal carbonyl group ($\text{C}=\text{O} \leftarrow \text{HNC}=\text{OH}^+ \rightarrow \text{S}$), with a distance of 2.00–2.05 Å from the proton attached to the *N*-acetyl carbonyl group to the S atom, and a distance of 2.09–2.14 Å from the H atom of the amide group to the O atom of the C-terminal carbonyl group. These conformers are further stabilized by the $\text{OH} \rightarrow \text{C}=\text{O}$ interaction of the carboxylic group with a distance of 2.36–2.37 Å between the carbonyl O and the hydroxyl H. Efficient charge and proton sharing among $-\text{COOH}$, $-\text{NH}$, protonated *N*-acetyl carbonyl, and sulfide results in cyclization of the structures of a–d through nine-membered rings.

Conformers e–n are stabilized by multiple hydrogen bonding within the carboxylic acid group and between the C-terminal carbonyl O and the amide H. However, these conformers adopt less preferred anti-configurations of the protonated *N*-acetyl group with regard to the side-chain sulfide, resulting in weaker charge delocalization and no hydrogen bonding with S. Consequently, conformers e–n lie 0.1–0.4 eV

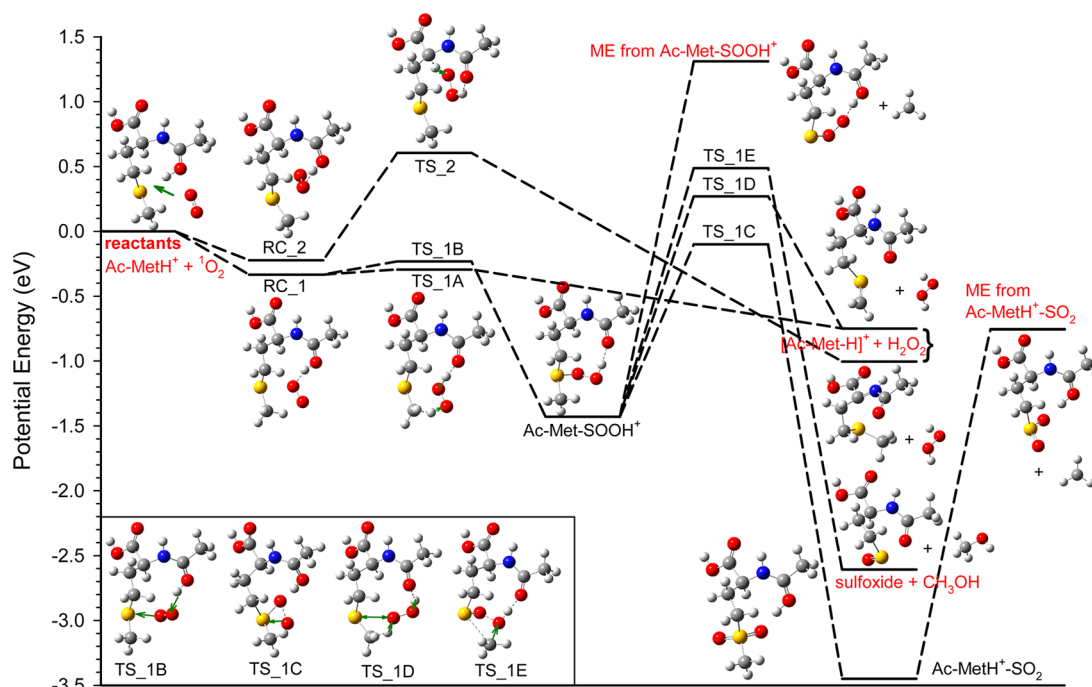


Figure 3. Schematic reaction coordinate for protonated *N*-acetyl methionine + $^1\text{O}_2$. Energies of complexes, TSs, and products, relative to reactants, are derived from B3LYP/6-31+G* values including ZPE. The bond distances are shown in angstroms.

higher in energy with respect to conformers a–d. The stable conformations we found are consistent with previous calculations which used a Monte Carlo simulation at the PM3 level to identify candidates for global minimum followed by optimization at B3LYP/6-31+G** and then single-point calculations at MP2/6-311+G(2d,p).⁴⁶

To verify the accuracy of the global minimum structure we identified, we have compared the proton affinity (PA) of conformer a with experimental value. The theoretical PA was calculated using the negative of the enthalpy of the protonation reaction via eq 1,

$$\text{PA} = E(\text{Ac-Met}) - E(\text{Ac-MetH}^+) + \frac{5}{2}RT \quad (1)$$

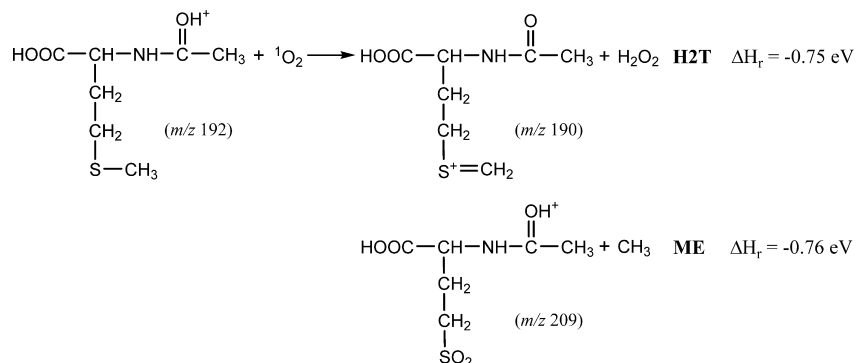
where $E(\text{Ac-MetH}^+)$ and $E(\text{Ac-Met})$ are the B3LYP/6-311+G(d,p) energies for conformer a and the corresponding neutral species, respectively, including ZPE corrections and thermal corrections, and $\frac{5}{2}RT$ represents the contributions from the proton translational energy ($\frac{3}{2}RT$) and $\Delta PV = RT$ (assuming ideal conditions).⁴⁶ The calculated PA for conformer a is 9.58 eV at 298 K, which is in good accord with the experimental value of 217.4 kcal/mol (=9.43 eV).⁴⁶

Among the Ac-MetH⁺ conformers presented in Figure 2, conformer a is predicted to have a population of 72% and conformers b–d account for a total population of 27%, while the remaining conformers have a total population of only 1% under our experimental condition. Therefore, conformer a was chosen as the reactant ion structure for construction of reaction coordinate and direct dynamics simulations. It is certainly possible that interconversion between various conformations might occur during collisions. It seems unlikely, however, that different conformations of Ac-MetH⁺ would significantly change the reaction coordinate, and our trajectory simulations of Ac-MetH⁺ + $^1\text{O}_2$ and MetH⁺ + $^1\text{O}_2$ ¹⁹ confirmed this conclusion.

2. Calculated Reaction Coordinate at Low E_{col} . Before presenting the calculated reaction coordinate, it is worth noting

that the excitation energy of triplet $^3\text{Ac-MetH}^+$ was calculated to be 3.1 eV. Consequently electronic energy transfer from $^1\text{O}_2$ + $^1\text{Ac-MetH}^+$ to $^3\text{O}_2$ + $^3\text{Ac-MetH}^+$ via intersystem crossing is 2.1 eV endothermic and could be overlooked over our collision energy range. The reactants therefore remain in singlet electronic states in reaction coordinate calculations. Figure 3 presents the potential energy surface (PES) associated with possible low-energy reaction pathways for Ac-MetH⁺ + $^1\text{O}_2$, with the reactants shown at zero energy. Energetics of complexes, TSs, and products are derived from B3LYP/6-31+G* calculations, except for that of TS_{1C} which was calculated at MP2/aug-cc-pVTZ and compared to the energy of the reactants at the same level of theory and basis set. The details of the geometries for complexes, TSs, and products are available by request to the corresponding author. Two weakly bound complexes (RC₁ and RC₂) and two covalently bound complexes (hydropersulfoxide Ac-Met-SOOH⁺ and sulfone Ac-MetH⁺-SO₂) were found. We have located TSs connecting the complexes to each other and to the products, as shown in Figure 3. Complexes RC₁ and ₂ could be characterized as reactant-like complexes, formed by electrostatic interaction and ionic hydrogen bonds. Both complexes have the O₂ moiety sandwiched between the protonated *N*-acetyl carbonyl group and the side chain. The binding energies of RC₁ and ₂ are 0.33 and 0.22 eV, respectively, with respect to the reactants. Because no rearrangement is required to form reactant-like complexes, it is unlikely that there would be significant activation barriers inhibiting formation of RC₁ and ₂. This was confirmed by relaxed potential energy scans running along the coordinate for dissociation of these complexes back to the reactants and by direct dynamics trajectory simulations to be discussed later. We note that, because of a lack of directional covalent bonds between Ac-MetH⁺ and O₂, RC₁ and ₂ do not have a well-defined geometry at the energies available in our experiment. These complexes are rather floppy, with a large amplitude of

Scheme 1



intermolecular motion and hence interconversion between each other. The point is that these complexes allow repeated encounters between the reactants, increasing reaction probability for collisions not initially in the correct geometry. To this extent, complexes RC_1 and _2 act as “precursor complexes” for reaction.

We first focus on the H2T channel. This channel corresponds to abstraction of two H atoms from Ac-MetH⁺ by ¹O₂, producing a dehydro compound [Ac-MetH - H]⁺ (*m/z* 190) and neutral H₂O₂. Complexes RC_1 and _2 have the right properties to serve as the precursors for H2T. DFT calculations suggest two H2T pathways, originating from each of these two precursors, respectively, and yielding two different structures of [Ac-MetH - H]⁺. One pathway appears to be reactants → RC_2 → TS_2 → CH₃CONH^αC(CO₂H)-CH₂CH₂SCH₃⁺ + H₂O₂, with concerted loss of H atoms from -^αCH and protonated *N*-acetyl carbonyl -C=OH⁺. The reaction enthalpy for this pathway is -1.00 eV; however, the high energy barrier associated with TS_2 (0.61 eV above the reactants) renders the contribution of this pathway negligible at low collision energies. An alternative route is reactants → RC_1 → TS_1A → CH₃CONHCH(CO₂H)CH₂CH₂SCH₂⁺ + H₂O₂. This pathway also requires transfer of two H atoms simultaneously, one from the protonated *N*-acetyl carbonyl -C=OH⁺ and the other from the side-chain methyl. This reaction has an enthalpy of -0.75 eV, and the associated activation barrier is 0.29 eV below the reactant energy, consistent with our experimental observation of an exothermic reaction for *m/z* 190.

The ME channel (i.e., formation of *m/z* 209 product ions) corresponds to a slightly more convoluted pathway; i.e., reactants → RC_1 → TS_1B → Ac-Met-SOOH⁺ → TS_1C → Ac-MetH⁺-SO₂ → CH₃COHNHCH(CO₂H)CH₂CH₂SO₂⁺ + CH₃. Reaction starts with formation of RC_1 and is followed by O₂ bonding with the S atom and simultaneous H abstraction by the dangling O atom from the neighboring protonated acetyl CH₃C=OH⁺ via TS_1B, leading to formation of a covalently bound hydropersulfoxide Ac-Met-SOOH⁺. The proton in Ac-Met-SOOH⁺ is shared by the *N*-acetyl carbonyl and persulfoxide groups but located closer to the persulfoxide group (1.00 Å) than to the *N*-acetyl carbonyl (1.62 Å). As a result, the -SOOH group carries most of the positive charge (more than 0.98) as measured by a Mulliken population analysis. Formation of an analogous hydropersulfoxide Met-SOOH⁺, accompanied by the shift of the protonation site, has been observed for the reaction of MetH⁺ + ¹O₂.¹⁹ Ac-Met-SOOH⁺ subsequently undergoes the cleavage of the O–O bond of -SOOH via TS_1C. During this structure rearrange-

ment, the departing O atom bonds with the S atom naturally, and the proton attached to this O returns to the *N*-acetyl carbonyl, leading to a sulfone compound Ac-MetH⁺-SO₂. Similar structure interconversion between hydropersulfoxide and sulfone has been recently reported for the reaction of 6-thioguanine with ¹O₂, yielding guanine-6-sulfonate.⁴⁹ Ac-MetH⁺-SO₂ may eliminate the side-chain CH₃ directly, forming a stable *m/z* 209 product ion CH₃COHNHCH(CO₂H)-CH₂CH₂SO₂⁺. The overall reaction enthalpy for formation of CH₃COHNHCH(CO₂H)CH₂CH₂SO₂⁺ + CH₃ is -0.76 eV. We have performed a relaxed potential energy surface scan running along the dissociating H₃C–S bond of Ac-MetH⁺-SO₂ using the B3LYP/6-31+G(d) method. The C–S bond length (*r*_{CS}) was continuously varied from 1.8 to 4.8 Å, and all coordinates other than *r*_{CS} were optimized at each point. The asymptotic energy of the resulting PES is approaching the ME product energy, suggesting methyl elimination from Ac-MetH⁺-SO₂ has no reverse barrier in excess of product energy and is facile.

Note that Ac-Met-SOOH⁺ may eliminate H₂O₂ via concerted elimination of -OOH and one of the side-chain methyl H atoms, producing H2T product ion CH₃CONHCH(CO₂H)CH₂CH₂SCH₂⁺. H₂O₂ elimination is common for allylic hydroperoxides in the presence of a labile H on a neighboring atom.^{50,51} However, the barrier TS_1D for this H₂O₂ elimination lies 0.27 eV above the reactants, suggesting that Ac-Met-SOOH⁺ may not be a good candidate for H2T at low *E*_{col}, as there exists a energetically more favorable H2T pathway that could proceed to the same products from RC_1 directly. In addition, we have ruled out the possibility of direct side-chain methyl elimination of Ac-Met-SOOH⁺, because the dissociation energy (1.31 eV above the reactants) is far too high to be driven by our collision energies.

In addition to H2T and ME, Figure 3 presents a product channel corresponding to elimination of a methanol molecule from Ac-MetH⁺-SO₂ via TS1_E, resulting in a sulfoxide ion CH₃CONHCH(CO₂H)CH₂CH₂SO⁺. The sulfoxide ion coincides in *m/z* with the reactant ion and therefore cannot be distinguished in product ion mass spectra. This product channel, albeit being exothermic by 2.61 eV, encounters a high activation barrier at TS_1E (0.49 eV above the reactants). It therefore cannot participate in the reaction at low *E*_{col} and is not considered further.

Overall, the most mechanistically important and energetically feasible reaction pathways at low *E*_{col} could be summarized as shown in Scheme 1. We cannot exclude the existence of additional reaction pathway(s) leading to *m/z* 190 and 209 product ions, but these two pathways are important at low *E*_{col}.

3. *RRKM Branching as a Probe of Complex-Mediate vs Direct Mechanism.* To evaluate whether the complexes and reaction pathways identified in Figure 3 could account for the experimental observations at low E_{col} , we have used the RRKM program to predict unimolecular kinetics of complexes RC_1, RC_2, and Ac-Met-SOOH⁺ as a function of E_{col} . Given that the harmonic frequencies associated with the rotation of the O₂ moiety within RC_1 and _2 are less than 100 cm⁻¹, it is certain that RC_1 and _2 interconvert rapidly compared to their lifetime. In that case, the ratio of density of states in RC_1 and _2 would give the information of which complex would have a more significant contribution to "statistical" reaction. It turns out that the DOS for RC_1 is an order of magnitude higher than that for RC_2. Since the precursor complex would predominantly exist in the structure of RC_1, we have therefore focused on dissociation rates and lifetimes of RC_1 and Ac-Met-SOOH⁺ only. All decomposition channels of RC_1 and Ac-Met-SOOH⁺ indicated by dashed lines in Figure 3 were included. No barrier is expected for decay of RC_1 back to reactants (i.e., no reaction) in excess of the asymptote; thus an orbiting transition state⁵² was assumed. Rotation quantum number K was treated as active in evaluating unimolecular rate constant $k(E, J)$ so that all $(2J + 1)$ K -levels are counted,⁵³ i.e.,

$$k(E, J) = \frac{d \sum_{K=-J}^J G[E - E_0 - E_r^\ddagger(J, K)]}{h \sum_{K=-J}^J N[E - E_r(J, K)]} \quad (2)$$

where d is the reaction path degeneracy, G is the sum of states from 0 to $E - E_0 - E_r^\ddagger$ at the transition state, N is the reactant density of states, E is the system energy, E_0 is the unimolecular dissociation threshold, and E_r and E_r^\ddagger are the rotational energies for the reactant and the transition state, respectively. The orbital angular momentum L was estimated from the collision cross section; i.e., $L = \mu v_{\text{rel}} (\sigma_{\text{col}}/\pi)^{1/2}$, where μ and v_{rel} are the reduced mass and relative velocity of collision partners, respectively. Complexes and TSs were described using scaled frequencies, polarizabilities, and momenta of inertia from DFT calculations.

As we discussed above, the mechanistic importance of RC_1 depends on its lifetime. If long enough lived, RC_1 could allow repeated encounters between two reactants, increasing the probability of eventually finding a low-energy path to Ac-Met-SOOH⁺. At E_{col} lower than 0.2 eV, the lifetime of RC_1 is 1–2 ps and drops quickly with increasing collision energy. Because of being trapped in a deep valley with high exit barriers, the lifetime of Ac-Met-SOOH⁺ is significantly longer than RC_1. We also calculated the "fly by" time required for a 5 Å motion of reactants at v_{rel} which are 0.84 ps at $E_{\text{col}} = 0.05$ eV and 0.6 ps at $E_{\text{col}} = 0.1$ eV. Therefore, the overall lifetime of the complexes is significantly longer than the fly by time. These complexes, if formed efficiently, could account for most of the collision times and conceivably have mechanistic significance at low E_{col} . At high energies, all complexes become insignificant because their lifetimes are too short for there to be any contributions.

If at low E_{col} the reaction is entirely complex-mediated and follows "statistical" decay of RC_1, the reaction efficiency could be determined by the branching ratios in decay of RC_1 "back to reactants" and "to H2T via TS_1A and Ac-Met-SOOH⁺ via TS_1B". RRKM calculations predict that at $E_{\text{col}} \leq 0.2$ eV the predominant decay channel for RC_1 corresponds to H2T and formation of Ac-Met-SOOH⁺, with a small branching back to the reactants (<12%). Assuming at low E_{col} Ac-Met-SOOH⁺ ultimately interconverts to Ac-MetH⁺-SO₂, followed by methyl

elimination, we estimate the total reaction efficiency > 88% at $E_{\text{col}} \leq 0.2$ eV. For comparison, the experimentally measured reaction efficiency is only 1% or less. Note that the RRKM-based model only gives the branching out of the set of complexes (RC_1 and _2) but omits consideration of the complex formation probability. A comparison of the RRKM-calculated branching ratio with experimental efficiency suggests that forming precursor complexes RC_1 and _2 accounts for only one-hundredth of all collisions at our lowest energy. The obvious implication is that most of the low- E_{col} collisions simply result in rebound of the reactants.

We need to note that one assumption we made in construction of the reaction coordinate is that the system is conserved in a singlet electronic state. This assumption is reasonable only when the reaction is adiabatic, i.e., no significant physical quenching of ¹O₂ would be involved. The large discrepancy between RRKM and experimental results is therefore not surprising in case physical quenching of ¹O₂ rather than chemical reaction dominates in collisions of Ac-MetH⁺ + ¹O₂. In that scenario, the ion–molecule collisions give rise to multiple states of the ion–molecule system, i.e., ¹Ac-MetH⁺ + ¹O₂ and ¹Ac-MetH⁺ + ³O₂.

4. *Direct Dynamics Trajectories Verified That Collisions Are Mostly Direct at Low E_{col} .* We have conducted direct dynamics trajectory simulations at $E_{\text{col}} = 0.05$ and 0.1 eV, respectively. The quasi-classic trajectory method we used is restricted to adiabatic collisions, i.e., it does not allow transitions from a singlet to a triplet state and therefore cannot reproduce physical quenching of ¹O₂. However, trajectories provide information concerning the early time collision dynamics where the electron spin of the reactants remains conserved.

We have recently reported quasi-classical trajectory simulations for CysH⁺ + ¹O₂³⁰ and CysH⁺(H₂O) + ¹O₂³³ at $E_{\text{col}} \leq 0.2$ eV. For both systems, most trajectories form precursor complexes and become trapped in that potential energy well, highlighting the importance of complex mediation at low-energy collisions. In fact, formation of precursor complexes is essential to their reactions. On the contrary, the majority (84–90%) of the Ac-MetH⁺ + ¹O₂ trajectories belong to direct, nonreactive scattering at E_{col} of 0.05–0.1 eV (i.e., fly by without forming any long-lasting complexes within the >1.3 ps simulation time), and only a few trajectories formed precursor complexes. Figure 4a demonstrates a trajectory representative of nonreactive collisions at $E_{\text{col}} = 0.1$ eV. The plots show the change in potential energy (PE) and CM distance as well as the approaching of the O₂ moiety toward the S atom (i.e., rSO and rSO') along the trajectory simulation time. The CM distance is the distance between the centers of mass of Ac-MetH⁺ and ¹O₂. The trajectory represents a direct scattering, with only one turning point in the relative motion of ¹O₂ vs Ac-MetH⁺; i.e., there is no sign of complex mediation. The time between the start of the trajectory and the onset of strong interaction, which depends on the reactant orientation, is around 350 fs. The time taken for reactants to approach within 5 Å of the CM distance is around 400 fs. During the trajectory, PE fluctuates due to the vibrational motions of the reactants.

Figure 4b illustrates a complex-forming trajectory. In this trajectory, ¹O₂ approaches the side-chain sulfide of Ac-MetH⁺, forming a loosely bound complex as shown by the decrease of the CM distance to less than 5 Å at 350 fs. After the initial collision, the precursor complex undergoes repeated structure interconversion between the collision partners, including

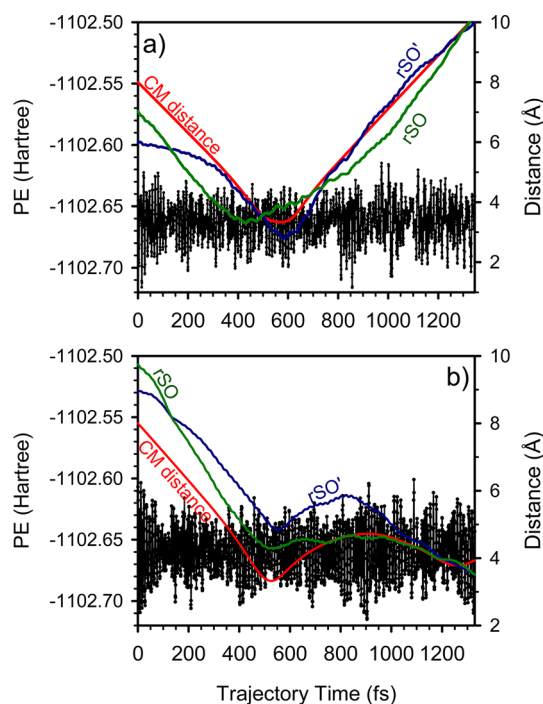


Figure 4. Representative plots of (a) a nonreactive trajectory and (b) a precursor complex-forming trajectory at $E_{\text{col}} = 0.10$ eV, showing the variations of potential energy, CM distance between Ac-MetH⁺ and ¹O₂ moieties, and two S–O bond lengths during the trajectory.

rotation of O₂ with respect to Ac-MetH⁺ as indicated by the oscillations of rSO and rSO'. The complex formed in the trajectory did not decay back to the reactants before the termination of the trajectory (1.3 ps), consistent with the RRKM-predicted complex lifetime. Note that precursor-complex-forming trajectories were observed only in collisions where the O₂ molecule attacks both the side chain and *N*-acetyl group of Ac-MetH⁺ simultaneously. Such restricted range of collision orientation (which was also observed in the trajectories of MetH⁺ + ¹O₂¹⁹) may bring about another dynamical bottleneck.

In summary, our trajectory results strongly support a direct collision mechanism at low E_{col} , which is not unreasonable considering the shallow potential wells that support precursor complexes. Direct collisions result in conversion of some collision energy into vibrational and rotational energy (i.e., $T \rightarrow E_{\text{int}}$). As mentioned above, the intersystem electronic energy transfer between ¹Ac-MetH⁺ + ¹O₂ and ³Ac-MetH⁺ + ³O₂ is not energetically accessible in our E_{col} range, but physical quenching of ¹O₂ could arise via electronic to vibrational energy transfer between reactants during direct collisions.⁵⁴

IV. CONCLUSION

Guided-ion-beam tandem mass spectrometry, in conjunction with DFT calculations, RRKM modeling, and quasi-classical trajectory simulations, was employed to probe the reaction dynamics between protonated *N*-acetylmethionine and ¹O₂ as well as the mechanistic origin of the extremely low reaction efficiency observed experimentally. The combined experimental and theoretical investigation reveals that only a small fraction of collisions undergo complex-mediated reactions, giving rise to CH₃CONHCH(CO₂H)CH₂CH₂SCH₂⁺ and H₂O₂ via hydrogen atom transfer, and CH₃COHNHCH(CO₂H)CH₂CH₂SO₂⁺ and CH₃ via methyl elimination from a sulfone intermediate

complex. The most probable collision events are direct scattering back to the reactants, accompanied by physical quenching of ¹O₂. Comparison of Ac-MetH⁺ + ¹O₂ vs MetH⁺ + ¹O₂ indicates the inhibition of the oxidation of the Met residue by an amide group, consistent with solution-phase photooxidation results. Present findings provide some insights, from mechanistic and kinetic points of view, to photooxidation of Met residues in peptides and proteins.

■ AUTHOR INFORMATION

Corresponding Author

*E-mail: jianbo.liu@qc.cuny.edu.

Notes

The authors declare no competing financial interest.

■ ACKNOWLEDGMENTS

This work was supported by the National Science Foundation CAREER Award (Grant No. CHE-0954507), Queens College Research Enhancement Funds, and PSC–CUNY Research Awards. We thank Alexander Greer (CUNY Brooklyn College) for his valuable comments on the manuscript.

■ REFERENCES

- (1) Davies, M. J. Singlet Oxygen-Mediated Damage to Proteins and Its Consequences. *Biochem. Biophys. Res. Commun.* **2003**, *305*, 761–770.
- (2) Davies, M. J. The Oxidative Environment and Protein Damage. *Biochim. Biophys. Acta* **2005**, *1703*, 93–109.
- (3) Palumbo, G. Photodynamic Therapy and Cancer: A Brief Sightseeing Tour. *Expert Opin. Drug Delivery* **2007**, *4*, 131–148.
- (4) Stadtman, E. R.; Remmen, H. V.; Richardson, A.; Wehr, N. B.; Levine, R. L. Methionine Oxidation and Aging. *Biochim. Biophys. Acta* **2005**, *1703*, 135–140.
- (5) Delaye, L.; Becerra, A.; Orgel, L.; Lazcano, A. Molecular Evolution of Peptide Methionine Sulfoxide Reductases (MsrA and MsrB): On the Early Development of a Mechanism That Protects against Oxidative Damage. *J. Mol. Evol.* **2007**, *64*, 15–32.
- (6) Schweitzer, C.; Schmidt, R. Physical Mechanisms of Generation and Deactivation of Singlet Oxygen. *Chem. Rev.* **2003**, *103*, 1685–1757.
- (7) Weil, L.; Gordon, W. G.; Buchert, A. R. Photooxidation of Amino Acids in the Presence of Methylene Blue. *Arch. Biochem.* **1951**, *33*, 90–109.
- (8) Spikes, J. D.; MacKnight, M. L. Dye-Sensitized Photooxidation of Proteins. *Ann. N. Y. Acad. Sci.* **1970**, *171*, 149–162.
- (9) Cohen, S. G.; Ojanpera, S. Photooxidation of Methionine and Related Compounds. *J. Am. Chem. Soc.* **1975**, *97*, S633–S634.
- (10) Sysak, P. K.; Foote, C. S.; Ching, T.-Y. Chemistry of Singlet Oxygen. XXV. Photooxygenation of Methionine. *Photochem. Photobiol.* **1977**, *26*, 19–27.
- (11) Rougee, M.; Bensasson, R. V.; Land, E. J.; Pariente, R. Deactivation of Singlet Molecular Oxygen by Thiols and Related Compounds, Possible Protectors against Skin Photosensitivity. *Photochem. Photobiol.* **1988**, *47*, 485–489.
- (12) Bertolotti, S. G.; Garcia, N. A.; Arguello, G. A. Effects of the Peptide Bond on the Singlet-Molecular-Oxygen-Mediated Sensitized Photo-Oxidation of Tyrosine and Tryptophan Dipeptides. A Kinetic Study. *J. Photochem. Photobiol., B* **1991**, *10*, 57–70.
- (13) Stadtman, E. R.; Berlett, B. S. Free-Radical-Mediated Modification of Proteins. *Free Radical Toxicol.* **1997**, 71–87.
- (14) Frimer, A. A. Reaction Modes and Products, Part 2. *Singlet O₂*, Vol. III; CRC Press: Boca Raton, FL, USA, 1985.
- (15) Jensen, F.; Greer, A.; Clennan, E. L. Reaction of Organic Sulfides with Singlet Oxygen. A Revised Mechanism. *J. Am. Chem. Soc.* **1998**, *120*, 4439–4449.

- (16) Bonesi, S. M.; Albini, A. Effect of Protic Cosolvents on the Photooxygenation of Diethyl Sulfide. *J. Org. Chem.* **2000**, *65*, 4532–4536.
- (17) Hug, G. L.; Bobrowski, K.; Kozubek, H.; Marciniak, B. Photooxidation of Methionine Derivates by the 4-Carboxybenzophenone Triplet State in Aqueous Solution. Intracomplex Proton Transfer Involving the Amino Group. *Photochem. Photobiol.* **1998**, *68*, 785–796.
- (18) Barata-Vallejo, S.; Ferreri, C.; Postigo, A.; Chatgililoglu, C. Radiation Chemical Studies of Methionine in Aqueous Solution: Understanding the Role of Molecular Oxygen. *Chem. Res. Toxicol.* **2010**, *23*, 258–263.
- (19) Fang, Y.; Liu, F.; Bennett, A.; Ara, S.; Liu, J. Experimental and Trajectory Study on Reaction of Protonated Methionine with Electronically Excited Singlet Molecular Oxygen ($a^1\Delta_g$): Reaction Dynamics and Collision Energy Effects. *J. Phys. Chem. B* **2011**, *115*, 2671–2682.
- (20) Criado, S.; Soltermann, A. T.; Marioli, J. M.; Garcia, N. A. Sensitized Photooxidation of Di- and Tripeptides of Tyrosine. *Photochem. Photobiol.* **1998**, *68*, 453–458.
- (21) Posadaz, A.; Biasutti, A.; Casale, C.; Sanz, J.; Amat-Guerri, F.; Garcia, N. A. Rose Bengal-Sensitized Photooxidation of the Dipeptides L-Tryptophyl-L-Phenylalanine, L-Tryptophyl-L-Tyrosine and L-Tryptophyl-L-Tryptophan: Kinetics, Mechanism and Photoproducts. *Photochem. Photobiol.* **2004**, *80*, 132–138.
- (22) Liu, J.; Zhang, F.; Zhao, Y.; Zhao, F.; Tang, Y.; Song, X. Influence of Peptide Bond on Photosensitized Oxidation of Tryptophan, Tyrosine and Histidine Dipeptides. *Chin. Sci. Bull.* **1997**, *42*, 1624–1628.
- (23) Criado, S.; Marioli, J. M.; Allegretti, P. E.; Furlong, J.; Nieto, F. J. R.; Martire, D. O.; Garcia, N. A. Oxidation of Di- and Tripeptides of Tyrosine and Valine Mediated by Singlet Molecular Oxygen, Phosphate Radicals and Sulfate Radicals. *J. Photochem. Photobiol., B* **2001**, *65*, 74–84.
- (24) Miskoski, S.; Garcia, N. A. Influence of the Peptide Bond on the Singlet Molecular Oxygen-Mediated ($O_2[^1\Delta]$) Photooxidation of Histidine and Methionine Dipeptides. A Kinetic Study. *Photochem. Photobiol.* **1993**, *57*, 447–452.
- (25) Straight, R.; Spikes, J. D. Sensitized Photooxidation of Amino Acids: Effects on the Reactivity of Their Primary Amine Groups with Fluorescamine and O-Phthalaldehyde. *Photochem. Photobiol.* **1978**, *27*, 565–569.
- (26) Michaeli, A.; Feitelson, J. Reactivity of Singlet Oxygen toward Amino Acids and Peptides. *Photochem. Photobiol.* **1994**, *59*, 284–289.
- (27) Marcus, R. A. Unimolecular Dissociations and Free-Radical Recombination Reactions. *J. Chem. Phys.* **1952**, *20*, 359–364.
- (28) Fenn, J. B.; Mann, M.; Meng, C. K.; Wong, S. F.; Whitehouse, C. M. Electrospray Ionization for Mass Spectrometry of Large Biomolecules. *Science* **1989**, *246*, 64–71.
- (29) Fang, Y.; Liu, J. Reaction of Protonated Tyrosine with Electronically Excited Singlet Molecular Oxygen: An Experimental and Trajectory Study. *J. Phys. Chem. A* **2009**, *113*, 11250–11261.
- (30) Liu, F.; Fang, Y.; Chen, Y.; Liu, J. Dissociative Excitation Energy Transfer in the Reactions of Protonated Cysteine and Tryptophan with Electronically Excited Singlet Molecular Oxygen ($a^1\Delta_g$). *J. Phys. Chem. B* **2011**, *115*, 9898–9909.
- (31) Liu, F.; Fang, Y.; Chen, Y.; Liu, J. Reactions of Deprotonated Tyrosine and Tryptophan with Electronically Excited Singlet Molecular Oxygen ($a^1\Delta_g$): A Guided-Ion-Beam Scattering, Statistical Modeling, and Trajectory Study. *J. Phys. Chem. B* **2012**, *116*, 6369–6379.
- (32) Fang, Y.; Liu, F.; Emre, R.; Liu, J. Guided-Ion-Beam Scattering and Direct Dynamics Trajectory Study on the Reaction of Deprotonated Cysteine with Singlet Molecular Oxygen. *J. Phys. Chem. B* **2013**, *117*, 2878–2887.
- (33) Liu, F.; Emre, R.; Lu, W.; Liu, J. Oxidation of Gas-Phase Hydrated Protonated/Deprotonated Cysteine: How Many Water Ligands Are Sufficient to Approach Solution-Phase Photooxidation Chemistry? *Phys. Chem. Chem. Phys.* **2013**, *15*, 20496–20509.
- (34) Ervin, K. M.; Armentrout, P. B. Translational Energy Dependence of $Ar^+ + XY \rightarrow ArX^+ + Y$ ($XY = H_2, D_2, HD$) from Thermal to 30 eV. *J. Chem. Phys.* **1985**, *83*, 166–189.
- (35) Midey, A.; Dotan, I.; Viggiano, A. A. Temperature Dependences for the Reactions of O^- and O_2^- with $O_2(a^1\Delta_g)$ from 200 to 700 K. *J. Phys. Chem. A* **2008**, *112*, 3040–3045.
- (36) Midey, A. J.; Dotan, I.; Viggiano, A. A. Reactions of $PO_xCl_y^-$ Ions with $O_2(a^1\Delta_g)$, H_2O , and Cl_2 at 298 K. *Int. J. Mass Spectrom.* **2008**, *273*, 7–10.
- (37) Lafferty, W. J.; Solodov, A. M.; Lugez, C. L.; Fraser, G. T. Rotational Line Strengths and Self-Pressure-Broadening Coefficients for the $1.27 \mu m, a^1\Delta_g - X^3\Sigma_g^-, \nu = 0 - 0$ Band of O_2 . *Appl. Opt.* **1998**, *37*, 2264–2270.
- (38) Troe, J. Statistical Adiabatic Channel Model of Ion-Neutral Dipole Capture Rate Constants. *Chem. Phys. Lett.* **1985**, *122*, 425–430.
- (39) Frisch, M. J.; Trucks, G. W.; Schlegel, H. B.; Scuseria, G. E.; Robb, M. A.; Cheeseman, J. R.; Scalmani, G.; Barone, V.; Mennucci, B.; Petersson, G. A.; et al. *Gaussian 09*, Rev. B. 01; Gaussian: Wallingford, CT, USA, 2009.
- (40) Zheng, J.; Alecu, I. M.; Lynch, B. J.; Zhao, Y.; Truhlar, D. G. Database of Frequency Scale Factors for Electronic Model Chemistries, Version 2; available at <http://comp.chem.umn.edu/freqscale/version2.htm>, 2010.
- (41) Zhu, L.; Hase, W. L. *A General RRKM Program (QCPE 644), Quantum Chemistry Program Exchange*; Chemistry Department, University of Indiana: Bloomington, IN, USA, 1993.
- (42) Hase, W. L.; Bolton, K.; de Sainte Claire, P.; Duchovic, R. J.; Hu, X.; Komornicki, A.; Li, G.; Lim, K.; Lu, D.; Peshlherbe, G. H.; et al. *Venus 99: A General Chemical Dynamics Computer Program*; Texas Tech University: Lubbock, TX, USA, 1999.
- (43) Peshlherbe, G. H.; Wang, H.; Hase, W. L. Monte Carlo Sampling for Classical Trajectory Simulations. *Adv. Chem. Phys.* **1999**, *105*, 177–201.
- (44) Bakken, V.; Millam, J. M.; Schlegel, H. B. Ab Initio Classical Trajectories on the Born-Oppenheimer Surface: Updating Methods for Hessian-Based Integrators. *J. Chem. Phys.* **1999**, *111*, 8773–8777.
- (45) Bacskay, G. B. A Quadratically Convergent Hartree-Fock (QC-SCF) Method. Application to Closed Shell Systems. *Chem. Phys.* **1981**, *61*, 385–404.
- (46) Lioe, H.; O'Hair, R. A. J.; Gronert, S.; Austin, A.; Reid, G. E. Experimental and Theoretical Proton Affinities of Methionine, Methionine Sulfoxide and Their N- and C-Terminal Derivatives. *Int. J. Mass Spectrom.* **2007**, *267*, 220–232.
- (47) Kemnitz, C. R.; Loewen, M. J. "Amide Resonance" Correlates with a Breadth of C–N Rotation Barriers. *J. Am. Chem. Soc.* **2007**, *129*, 2521–2528.
- (48) Leach, A. R. *Molecular Modeling: Principles and Applications*; Pearson, Prentice Hall: Harlow, England, 2001.
- (49) Zou, X.; Zhao, H.; Yu, Y.; Su, H. Formation of Guanine-6-Sulfonate from 6-Thioguanine and Singlet Oxygen: A Combined Theoretical and Experimental Study. *J. Am. Chem. Soc.* **2013**, *135*, 4509–4515.
- (50) Chen, Y.-Z.; Wu, L.-Z.; Peng, M.-L.; Zhang, D.; Zhang, L.-P.; Tung, C.-H. Synthesis of α,β -Unsaturated γ -Lactones Via Photooxygenation of 2,3-Dihydrofurans Followed by Ferrous Ion-Catalyzed gem-Dehydration. *Tetrahedron* **2006**, *62*, 10688–10693.
- (51) Morgan, P. E.; Dean, R. T.; Davies, M. J. Protective Mechanisms against Peptide and Protein Peroxides Generated by Singlet Oxygen. *Free Radicals Biol. Med.* **2004**, *36*, 484–496.
- (52) Rodgers, M. T.; Ervin, K. M.; Armentrout, P. B. Statistical Modeling of Collision-Induced Dissociation Thresholds. *J. Chem. Phys.* **1997**, *106*, 4499–4508.
- (53) Zhu, L.; Hase, W. L. Comparison of Modes for Calculating the RRKM Unimolecular Constant $K(E,J)$. *Chem. Phys. Lett.* **1990**, *175*, 117–124.
- (54) Wilkinson, F.; Helman, W. P.; Ross, A. B. Rate Constants for the Decay and Reactions of the Lowest Electronically Excited Singlet State of Molecular Oxygen in Solution. An Expanded and Revised Compilation. *J. Phys. Chem. Ref. Data* **1995**, *24*, 663–1021.